Molecular Therapy
Oncolytics
Original Article

Enhanced Therapeutic Efficacy of a Novel Oncolytic Herpes Simplex Virus Type 2 Encoding an Antibody Against Programmed Cell Death 1

Yujie Zhu,[1,5] Xiao Hu,[1,5] Lin Feng,[1] Zhenrong Yang,[1] Lulin Zhou,[1] Xinchun Duan,[2] Shujun Cheng,[1] Wen Zhang,[3] Binlei Liu,[4] and Kaitai Zhang[1]

[1]State Key Laboratory of Molecular Oncology, National Cancer Center/National Clinical Research Center for Cancer/Cancer Hospital, Chinese Academy of Medical Sciences and Peking Union Medical College, Beijing 100021, China; [2]Department of Thoracic Surgery, Beijing Chest Hospital, Capital Medical University, Beijing 101149, China; [3]Department of Immunology, National Cancer Center/National Clinical Research Center for Cancer/Cancer Hospital, Chinese Academy of Medical Sciences and Peking Union Medical College, Beijing 100021, China; [4]National "111" Centre for Cellular Regulation and Molecular Pharmaceutics, Key Laboratory of Fermentation Engineering (Ministry of Education), Hubei Provincial Cooperative Innovation Center of Industrial Fermentation, Hubei Key Laboratory of Industrial Microbiology, Hubei University of Technology, Wuhan 430068, Hubei, China

The efficacy of immune checkpoint blockade therapy against immunologically "cold" tumors can be enhanced by applying the checkpoint inhibitors in combination with oncolytic viruses. Alternatively, the oncolytic virus construct has been modified to express factors that boost oncolytic virus function. We engineered a novel oncolytic herpes simplex virus 2 (HSV2) encoding an anti-human programmed cell death 1 (PD-1) monoclonal antibody (oHSV2-aPD1). This virus resulted in the detectable expression of a functional monoclonal antibody against human PD-1 by infecting eukaryotic cells. Therapeutic efficacy of oHSV2-aPD1 proved superior to unmodified oncolytic HSV2 treatment or PD-1 blockade alone and as effective as their combination in the poorly immunogenic melanoma models. Additionally, local oHSV2-aPD1 treatment induced a durable antitumor response and activated many immune effector cells and molecules both in the tumor microenvironment and in the systemic immune system. This provides support for combinatorial strategies involving local administration of an oncolytic HSV2 expressing a PD-1 inhibitor.

INTRODUCTION

Immune checkpoint blockade (ICB), one of the most important advances in the history of cancer treatment, uses antibodies to disrupt interactions between suppressive receptors on T cells and their inhibitory ligands on tumor cells. Particular targets of interest include cytotoxic T lymphocyte-associated antigen 4 (CTLA-4), programmed cell death 1 (PD-1), and programmed cell death 1 ligand 1 (PD-L1). ICB has achieved inspiring clinical responses in a subset of patients with various tumor types.[1–4] At present, the US Food and Drug Administration (FDA) has approved six antibodies against CTLA-4, PD-1, or PD-L1 for 12 cancer indications.[5] Among these, it should be noted that the PD-1 antibodies pembrolizumab and nivolumab are the first class of agents to be used in cancers with high microsatellite instability (MSI-h), a classification based on a genetic characteristic other than the origin of the cancers' tissue.[6] Unfortunately, only about 10%–40% of patients with certain tumors will benefit from checkpoint blockade therapy.[1–3,7,8]

The poor efficacy of PD-1/PD-L1 blockade is often attributed to low tumor mutational burden, low/no tumor cell PD-L1 expression, and limited infiltration of effector T cells into the tumor microenvironment (TME).[9–11] In addition, the intravenous application of immune checkpoint inhibitors not only limits the effective dose of antibody that reaches the tumor lesions but also causes mechanism-related toxicity due to tissue-specific inflammation.[1–4,7,8] Thus, additional approaches will be required to design combinatorial strategies that will enhance and extend therapeutic efficacy to a larger patient population and acquire synergistic, durable clinical responses against a broad range of cancer types.

Oncolytic viruses (OVs), which are native or genetically engineered to selectively replicate within neoplastic cells, represent

Received 26 September 2019; accepted 13 October 2019;
https://doi.org/10.1016/j.omto.2019.10.003.

[5]These authors contributed equally to this work.

Correspondence: Kaitai Zhang, State Key Laboratory of Molecular Oncology, National Cancer Center/National Clinical Research Center for Cancer/Cancer Hospital, Chinese Academy of Medical Sciences and Peking Union Medical College, No. 17, Panjiayuannanli, Chaoyang District, Beijing 100021, China
E-mail: Zhangkt@cicams.ac.cn
Correspondence: Binlei Liu, National "111" Centre for Cellular Regulation and Molecular Pharmaceutics, Key Laboratory of Fermentation Engineering (Ministry of Education), Hubei Provincial Cooperative Innovation Center of Industrial Fermentation, Hubei Key Laboratory of Industrial Microbiology, Hubei University of Technology, Wuhan 430068, Hubei, China.
E-mail: 1836035949@qq.com
Correspondence: Wen Zhang, Department of Immunology, National Cancer Center/National Clinical Research Center for Cancer/Cancer Hospital, Chinese Academy of Medical Sciences and Peking Union Medical College, Beijing 100021, China.
E-mail: zhangwen@cicams.ac.cn

another novel group of promising immunotherapeutic agents for cancer treatment. The antitumor response to OVs results from a dual mechanism involving both direct lytic activity against tumor cells and indirect induction of innate and adaptive antitumor immunity.[12] A variety of OVs have been evaluated in clinical trials for their safety and efficacy in advanced solid tumors.[13–16] Further, a number of preclinical studies have demonstrated that OVs can enhance the efficacy of ICB in a range of tumor models.[17–20] Recently, a phase Ib clinical study[21] demonstrated that a combination of talimogene laherparepvec (T-VEC, a modified herpes simplex virus 1 encoding human granulocyte-macrophage colony-stimulating factor) and pembrolizumab (typically used for melanoma treatment) led to an increase in tumor-infiltrating lymphocytes (TILs), particularly interferon-γ (IFN-γ)-producing $CD8^+$ T cells. Furthermore, PD-L1 expression was upregulated in the TME following T-VEC treatment. It appears that T cell recruitment and interferon production during OV-mediated lysis induce susceptibility to ICB in previously resistant tumors.[22]

To maximize the local effective dose of checkpoint inhibitors and acquire synergistic therapeutic efficacy, we sought to construct a novel OV: oncolytic herpes simplex virus 2 (HSV2) encoding an anti-human PD-1 monoclonal antibody (oHSV2-aPD1). Through local injection of oHSV2-aPD1, the anti-human PD-1 monoclonal antibody (anti-hPD1mAb) can be delivered directly to the tumor site, thus minimizing the toxicity that typically accompanies checkpoint blockade therapy. Here, we found that oHSV2-aPD1 exerted a compelling antitumor effect in a PD-1-humanized mouse melanoma model by secreting an antibody against human PD-1. This treatment was superior to either unarmed oncolytic HSV2 (oHSV2) treatment or PD-1 blockade alone. Additionally, localized oHSV2-aPD1 application induced an antitumor memory and activated immune effector cells and molecules both in the TME and in the immune system as a whole. This provides support for combinatorial strategies involving local administration of an oncolytic HSV2 expressing a PD-1 inhibitor.

RESULTS

oHSV2-aPD1 Expresses a Functional Anti-hPD1mAb by Infecting Eukaryotic Cells

We engineered the oHSV2 such that the major neurovirulence gene, infected cell protein 34.5 (ICP34.5), was removed in order to attenuate resistance to interferon in normal cells. Infected cell protein 47 (ICP47) was deleted in order to enhance the expression of major histocompatibility complex (MHC) class I in infected cells, which could promote the presentation of tumor-associated antigens (TAAs), as reported in our previous study.[23] oHSV2-aPD1 was developed from oHSV2. The coding sequence for the monoclonal antibody (mAb) against human PD-1, which was designed using publicly available heavy and light chain (BMS-936558) sequences, was introduced into the ICP34.5 locus (Figure 1A). The partial anti-hPD1mAb was completed using the B cell antigen receptor signal sequence, with the heavy chain driven by the cytomegalovirus (CMV) promoter and the light chain under the control of the Rous sarcoma virus long terminal repeat (RSV LTR). The HG52 laboratory strain was selected as the parental virus because of its decreased virulence in comparison with other HSV2 strains.[24] Viral structures were confirmed by PCR (Figure S1A) and sequencing of modified regions.

In preliminary tests, Vero cells, a permissive and productive cell line, were infected with oHSV2-aPD1. Western blotting of culture supernatants purified with protein G agarose under denaturing conditions demonstrated that infected cells expressed the approximately 55-kDa heavy chain and the approximately 26-kDa light chain (Figure 1B). Expression tests were also performed using three other eukaryotic cell lines (CT26, B16R and A549); results in these cell lines recapitulated those in Vero cells (Figures 1B and 1C; Figure S1B), suggesting that both murine and human neoplastic cells can correctly encode the anti-hPD1mAb.

To explore whether the secreted anti-hPD1mAb could bind to the immune checkpoint PD-1, we analyzed a commercial recombinant human PD-1 with a C-terminal polyhistidine tag (His-tag) by immunoblotting. The results demonstrated that the antibody produced by oHSV2-aPD1-infected CT26 cells was able to bind with the recombinant PD-1 protein. The primary antibody was explicitly recognized by the horseradish peroxidase (HRP)-conjugated goat anti-human IgG (H+L) secondary antibody (Figure 1D).

To further verify that the virally expressed anti-hPD1mAb was capable of blocking signaling through the PD-1 pathway, we collected culture supernatants from virus-infected cells and added them to peripheral blood mononuclear cells (PBMCs) in patients with advanced solid tumors.[25] In all eight cases (Table S1), anti-hPD1mAb antagonized cell surface PD-1, thus freeing and activating T cells, which was observed as an enhancement in IFN-γ (Figures S2A and S2C) and interleukin-2 (IL-2) (Figures S2B and S2D) production compared with the oHSV2 group. Some variations in this effect were observed in different patients. This may be attributed to different degrees of immunosuppression in PBMC samples and diverse tumor-immunosuppressive mechanisms.

Taken together, these results indicated that infection of tumor cells with oHSV2-aPD1 resulted in the detectable expression of a functional mAb against human PD-1, which caused T cell activation, as measured by IFN-γ and IL-2 levels.

Oncolytic Spectrum and Oncolytic Activity of oHSV2-aPD1 *In Vitro*

The infectious and oncolytic activities of oHSV2-aPD1 were compared with those of oHSV2 in order to evaluate the influence of the different transgenes on the virus properties. B16F10 cells, which lack an HSV receptor, were poorly infected by both

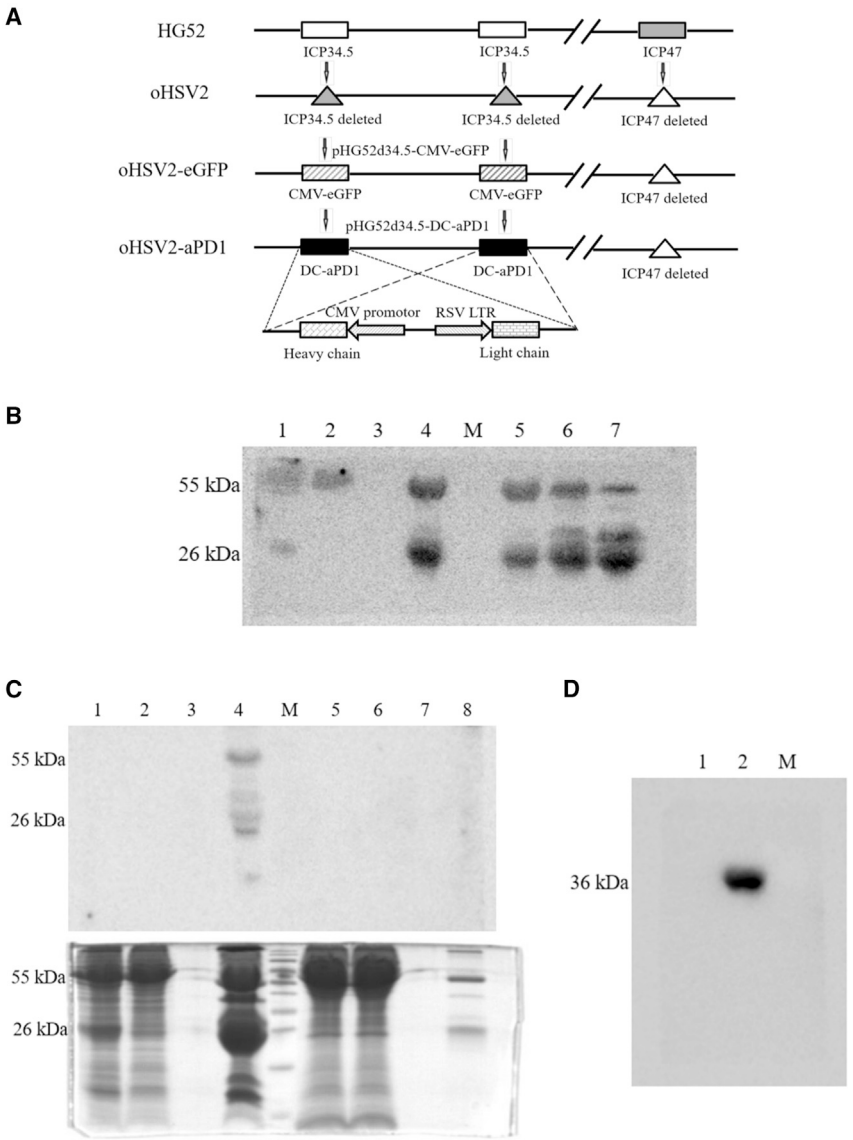

Figure 1. Evaluation of oHSV2-aPD1-Induced Anti-hPD1mAb Expression and Function

(A) Schematic of oHSV2 and oHSV2-aPD1 construction. Both oHSV2 and oHSV2-aPD1 were derived from the HG52 laboratory strain with the ICP34.5 and ICP47 genes deleted. To construct oHSV2-aPD1, the ICP34.5 locus was replaced by the anti-hPD1mAb encoding sequence. Heavy chain expression was driven by the CMV promoter, whereas light chain expression was driven by the RSV LTR. (B) Culture supernatants were collected from oHSV2-aPD1-infected A549 (lanes 1–5), Vero (lane 6), or CT26 (lane 7) cells, purified using protein G agarose, and loaded on SDS-PAGE gels under denaturing conditions. Lane 1: culture supernatant before purification, lane 2: supernatant after purification, lane 3: washing buffer from purification steps, lanes 4–7: purification eluent. (C) Culture supernatants were recovered from B16R cells infected with oHSV2-aPD1 (lanes 1–4) or mock infected (lanes 5–8), purified using protein G agarose, and loaded on SDS-PAGE gels under denaturing conditions. Upper panel: image following transfer onto PVDF membrane. Lower panel: matched image of the gel stained with Coomassie brilliant blue. Lanes 1 and 5: culture supernatant before purification, lanes 2 and 6: supernatant after purification, lanes 3 and 7: washing buffer from purification, and lanes 4 and 8: purification eluent. (D) A His-tagged protein of approximately 32 kDa (lane 1, negative control) and a His-tagged commercially available recombinant extracellular domain of human PD-1 (36 kDa) (lane 2) were loaded on an SDS-PAGE gel and then incubated with the anti-hPD1mAb produced by oHSV2-aPD1-infected CT26 followed by HRP-conjugated goat anti-human IgG (H+L). M, molecular marker.

viruses. In contrast, B16R (derived from B16F10 cells stably transfected with herpes virus entry mediator [HVEM]),[26] CT26, and 4T1 cells were equally well infected by both oHSV2 and oHSV2-PD1, suggesting that the two kinds of viruses had a similar spectrum of infection in the tested cell lines (Figure 2A). We also observed the same phenomena in a panel of human tumor cell lines originating from the lung, esophagus, stomach, liver, rectum, brain, thyroid, ovary, kidney, tongue, and pharynx (Figure S3).

We also evaluated the selective oncolytic activity of each virus at three multiplicities of infection (MOIs). Results showed that at low (MOI = 0.1) and high (MOI = 5) doses, the two viruses had similar oncolytic abilities in both murine and human tumor cells. At a medium MOI (MOI = 1), however, oHSV2-aPD1 demonstrated increased impairment of cell viability in several cell lines (such as B16R, CT26, 4T1, A549, U373, SKOV3, HT29, and BGC823) (Figure 2B; Figure S4). In addition, the oncolytic activity of the same virus widely varied in different kinds of cell lines. Both viruses were relatively ineffective in B16F10 cells (Figure 2B) and white blood cells (WBCs) (Figure S4) due to a lack of infectious routes. Interestingly, we also found that both viruses slightly stimulated WBC proliferation at low and medium MOIs, which may contribute to their antitumor effects.

In summary, compared with those of oHSV2, the viral infection and oncolytic sensitivity of oHSV2-aPD1 were unimpaired by the transgenes.

Application of oHSV2-aPD1 Improves the Antitumoral Efficacy of oHSV2 in the Implanted Poorly Immunogenic B16R Melanoma Model

To determine whether the anti-hPD1mAb vector could enhance antitumoral efficacy, we evaluated tumor growth and survival rates

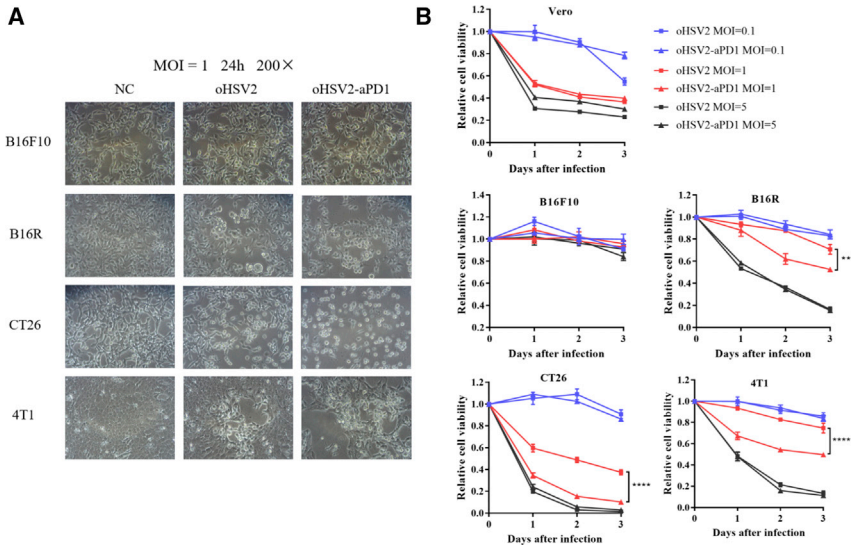

Figure 2. Infectious and Oncolytic Activities of oHSV2 and oHSV2-aPD1 *In Vitro*

(A) oHSV2 or oHSV2-aPD1 were used to mock infect (negative control [NC]) or infect murine tumor cells, including B16F10, B16R, CT26, and 4T1 at MOI = 1 for 24 h. Images were collected at 20× objective magnification with an inverted phase-contrast microscope. (B) oHSV2 or oHSV2-aPD1 were used to mock infect or infect Vero, B16F10, B16R, CT26, and 4T1 cells at the three indicated MOIs for the indicated lengths of time. Data are presented as the mean ± SD of three measurements. Statistical significance is indicated by **$p < 0.01$ and ****$p < 0.0001$.

of the B16R C57BL/6J-Pdcd1 mouse melanoma model, which has a humanized PD-1. The tumor-bearing mice were treated with PBS, oHSV2, or oHSV2-aPD1 every other day via intratumoral injection beginning when the tumor average diameter reached 5 mm (Figure 3A). For survival analyses, animals were monitored for 64 days beginning from the day of B16R inoculation in the right flank. As expected, both oHSV2 and oHSV2-aPD1 inhibited tumor growth ($p < 0.0001$) and prolonged the survival ($p < 0.0001$) of mice relative to PBS treatment (Figures 3B–3D). It should be noted that, although there was no statistically significant difference ($p = 0.079$) in survival between the oHSV2 and oHSV2-aPD1 groups, oHSV2-aPD1 administration did result in an improved trend of tumor-free survival (0% for PBS, 30% for oHSV2, and 50% for oHSV2-aPD1).

We also performed the same experiments in normal C57BL/6J mice and found that there was no significant difference in tumor burden ($p = 0.48$) or survival time ($p = 0.73$) between oHSV2 and oHSV2-aPD1 groups (Figures S5A–S5D), suggesting that local injection of oHSV2-aPD1 allowed for the intratumoral expression of anti-hPD1mAb, thus enhancing the therapeutic efficiency in humanized-PD-1 mice.

Via selective replication within neoplastic cells, localized OV treatment resulted in a lytic effect leading to the release of TAAs. These TAAs improved the function of antigen-presenting cells, leading to the activation of tumor-specific T cell responses in the TME,[27] as well as in peripheral immune organs due to lymphocyte homing. To support this hypothesis, we isolated splenic lymphocytes from mice following treatment completion. Lymphocytes were then cocultured with the homologous B16R cells *in vitro*. We found that the primed specific T cells could target and kill B16R tumor cells (Figures 3E and 3F), consistent with the therapeutic effects observed *in vivo*. In addition, we also observed that cytotoxicity correlated with the treatment dose established using the effector-target ratio (Figure 3F).

These data demonstrate that oHSV2-aPD1 is superior to oHSV2 in terms of reductions in tumor burden and increase in survival benefits.

Local oHSV2-aPD1 Application Induces a Massive Elevation of Immune Effector Cells and Downregulation of Immunosuppressive Cells in the Spleen

OV antitumor effects stem from both direct oncolysis and initiation of antitumor immunity. To determine the cellular and molecular mechanisms responsible for the identified therapeutic effect, we collected and processed mouse spleens 5 days after therapeutic completion for flow cytometry analysis. Treatment with oHSV2-aPD1 led to increased percentages of $CD4^+$ T cells, $CD8^+$ T cells, and $CD3^+$ T cells. Meanwhile, oHSV2 treatment resulted in only increased $CD8^+$ T cells compared with the control group (PBS) (Figures 4A–4C). Interestingly, NK cells, one of the agents of innate immunity, declined in the oHSV2-aPD1 group (Figure 4D), suggesting an impaired antiviral effect. We also determined the $CD44^+$ proportion of $CD4^+$ and $CD8^+$ T cells, which indicates antigen-primed or effector memory T cells (Tems),[28] and we found that both $CD4^+$ and $CD8^+$ memory T cells increased significantly following OV treatments (Figures 4E and 4F). Moreover, the percentage of dendritic cells (DCs) was also enhanced in the OV groups (Figure 4G). However, we observed an upregulation of the inducible costimulator (ICOS) expression in $CD8^+$ T cells only in the oHSV2-aPD1 group (Figure 4H). We also explored the intracellular secretion of IL-2, IFN-γ, and tumor necrosis factor alpha (TNF-α) in $CD8^+$ T cells. Results demonstrated that activated T cell percentages were increased following oHSV2-aPD1 treatment (Figures 4I–4K). Ki67, a proliferation marker in $CD8^+$ T cells, was enhanced significantly in both virus groups relative to the PBS-treated group (Figure 4L), further supporting our hypothesis of adoptive antitumor immunity.

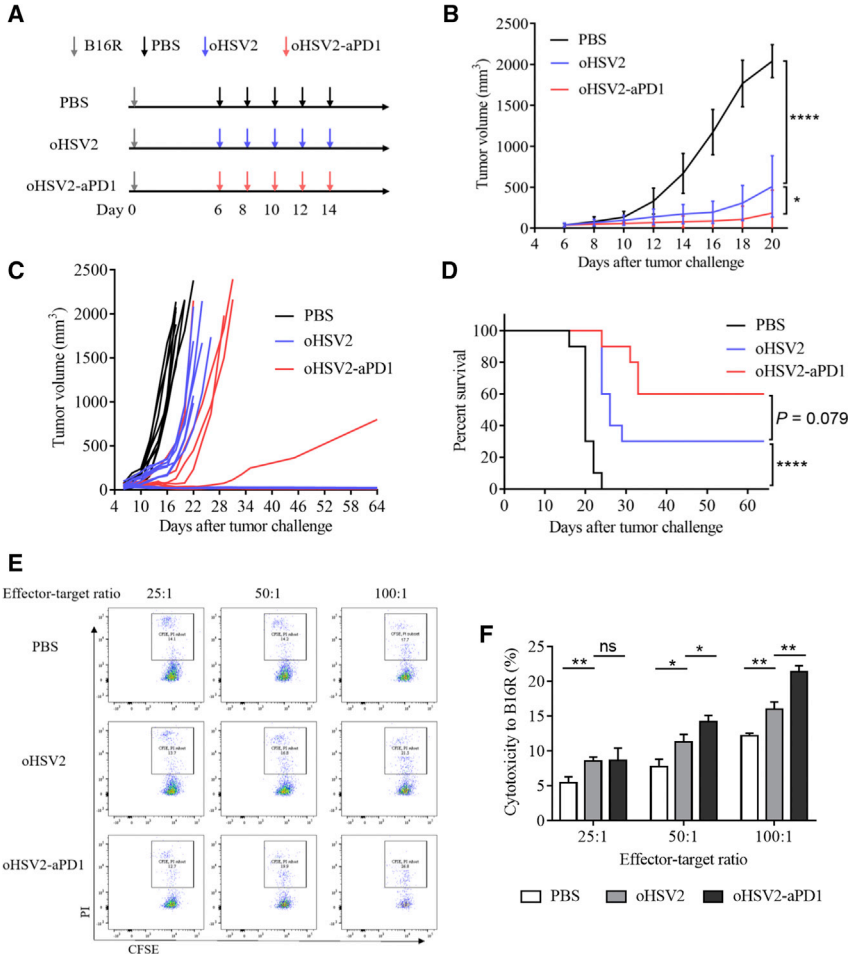

Figure 3. Therapeutic Effects of oHSV2-aPD1 in a B16R Melanoma Model

C57BL/6J-Pdcd1 mice were subcutaneously inoculated with 2×10^5 B16R cancer cells and treated via intratumoral injection as described in the Materials and Methods (n = 10 per group). (A) Schematic representation of the experiment. (B) Tumor volumes were measured every other day, and data are presented as the mean ± SD. (C) Tumor volumes are presented as individual measurements. (D) The overall survival of tumor-bearing mice is illustrated by Kaplan-Meier curves and was analyzed using the log rank test. (E and F) Mice were euthanized five days after treatment. Splenic lymphocytes were isolated and cocultured with B16R cells at the indicated ratios for 6 h and then harvested to test cytotoxic efficiency by flow cytometry. (E and F) Representative data (E) and statistical results (the measured value of samples minus the natural mortality rate of B16R) (F) from three independent samples. Mean ± SD is shown. *p < 0.05, **p < 0.01, ****p < 0.0001. ns, not significant.

To further characterize the mechanisms of OV-stimulated antitumor effects, we also investigated changes in regulatory T cells (Tregs), myeloid-derived suppressor cells (MDSCs), and $CD11b^+F4/80^+$ cells. Treg and MDSC levels were not decreased in the oHSV2-aPD1 group compared with the oHSV2 group but were significantly reduced compared with the PBS group (Figures 5A and 5B). oHSV2 treatment did not have any effect on the percentage of $CD11b^+F4/80^+$ cells, whereas oHSV2-aPD1 treatment resulted in a significantly reduced $CD11b^+F4/80^+$ cell proportion (Figure 5C). We then studied the impact of OV treatments on four coinhibitory molecules expressed on $CD8^+$ cells. oHSV2 led to a reduction in CTLA-4 expression ($p < 0.05$), whereas oHSV2-aPD1 led to an even more significant decrease ($p < 0.01$) compared with the PBS group (Figure 5D). No significant differences were observed in T cell immunoglobulin mucin 3 (TIM-3) and lymphocyte activation gene 3 (LAG-3) levels between the oHSV2 and oHSV2-aPD1 groups. However, when compared with the PBS treatment group, both OVs led to a significant reduction in the levels of these molecules (Figures 5E and 5F). No significant changes were observed in the levels of T cell immunoglobulin and ITIM domain (TIGIT) expression among all groups, although there was a decreasing trend observed in the group treated with oHSV2-aPD1 (Figure 5G).

Together, these results reveal that local application of oHSV2-aPD1 leads to powerful systemic antitumor immunity by enhancing the proportion of effector cells and reducing the percentage of immunosuppressive cells.

oHSV2-aPD1 Treatment Alone Exerts Similar Antitumor Effects as the Dual Therapy

To further dissect the therapeutic effect of anti-hPD1mAb expressed by oHSV2-aPD1, we compared this treatment with the dual therapy that unarmed oHSV2 plus anti-human PD-1 antibody (anti-PD1). In the B16R melanoma model, both anti-PD1- and oHSV2-treated mice exhibited decreased tumor burden compared with isotype-treated mice. Meanwhile, the combined treatments, oHSV2-aPD1 alone or oHSV2 plus anti-PD1, led to statistically significant improvements in tumor inhibition compared with the mono-therapies (Figures 6A–6C). Treatment with anti-PD1 or oHSV2 improved survival times; however, the oHSV2-aPD1 therapy led to the best therapeutic effect (Figure 6D).

We then rechallenged the 10 tumor-free mice from the four kinds of immunotherapies (anti-PD1, n = 1; oHSV2, n = 2; oHSV2-aPD1, n = 4; oHSV2 + anti-PD1, n = 3), except for the isotype group at day 64, with the same quantity of B16R in the contralateral flank. Our data showed that, within the 35-day observation period following B16R reinoculation, none of the tumor-free mice suffered melanoma reoccurrence, whereas all mice from the naive control group experienced tumor occurrence 11 days later (Figure S6). This indicated that all immunotherapies (PD-1 blockade alone, oHSV2 alone, or combined treatments) led to an antitumor immune memory.

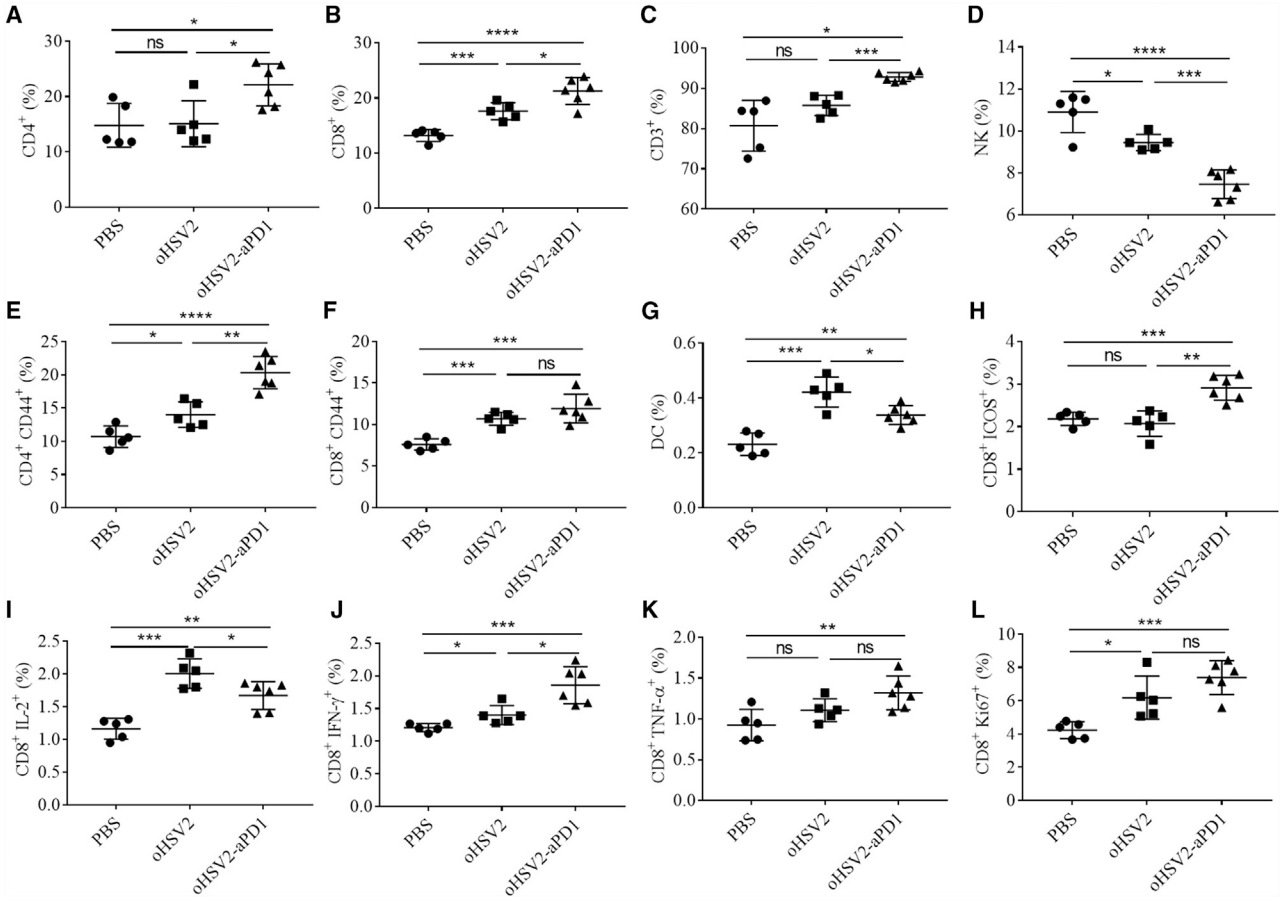

Figure 4. oHSV2-aPD1 Treatment Facilitates Amplification of Immune Effector Cells in the Spleen

C57BL/6J-Pdcd1 mice were subcutaneously inoculated with 2×10^5 B16R cancer cells and treated with oHSV2 or oHSV2-aPD1 as described in the Materials and Methods. Single cells were isolated from spleens collected 5 days after the last treatment. (A–L) These cells were incubated with CD16/32 antibody and stained with antibodies to determine quantities of T cells (A–C), NKs (defined as $CD3^-NK1.1^+$) (D), memory T cells (defined as $CD4^+CD44^+$ or $CD8^+CD44^+$) (E and F), DCs (defined as $CD45^{+-}CD11b^+CD11c^+Ly6G^-$) (G), and $CD8^+$ T cell activation (H–L). Data are presented as individual replicates. *$p < 0.05$, **$p < 0.01$, ***$p < 0.001$, ****$p < 0.0001$. ns, not significant.

Overall, our data suggest that treatment with a vectorized form of PD-1 antibody in the oHSV2 virus is as effective as the combination with an unarmed oHSV2 and systemic anti-PD1 administration, and that this treatment method induces a memory response against tumor.

Local Administration with oHSV2-aPD1 Induces Activated Immune Effectors Both in the TME and the Systemic Immune System

To examine the B16R TME and systemic immune system in the treated animals, we collected and processed tumor and spleen tissues for analysis of the transcriptome by next generation sequencing (NGS). Principal-component analysis (PCA) of the expressed genes indicated that the transcriptomic features of tumor tissues correlated with the different therapies (Figure 7A, left circles). In the spleen tissues, samples clustered by similar curative effects, whereas distinct effects were obviously separated by the boundary PC2 = 0 (Figure 7A, right circles). These results indicated that systemic antitumor immunity responding to the splenic transcriptome might play a key role in antitumor effects.

Next, we performed a detailed analysis of the immune profile based on 770 genes (derived from the database NanoString); the results of this analysis showed similar phenomena. As shown in Figure 7B, the anti-PD1 group displayed similar immune features to the isotype group in tumor tissues, whereas the virus groups were distinctly different, suggesting that intratumoral injection of OVs, especially oHSV2-aPD1, caused drastic changes in the TME. In spleen tissues (Figure 7B), the expression of immune-related genes was correlated with curative outcomes; i.e., samples with improved outcomes were distinctly different from those with worse outcomes, even with the same treatments. This phenomenon was particularly evident in the anti-PD1 group. Specifically, most immune effectors were activated in the tumor tissues from the oHSV2-aPD1 group relative to the control group. These effectors contributed to antigen processing and presentation (B cells, DCs, MHC class I and II, etc.), immune

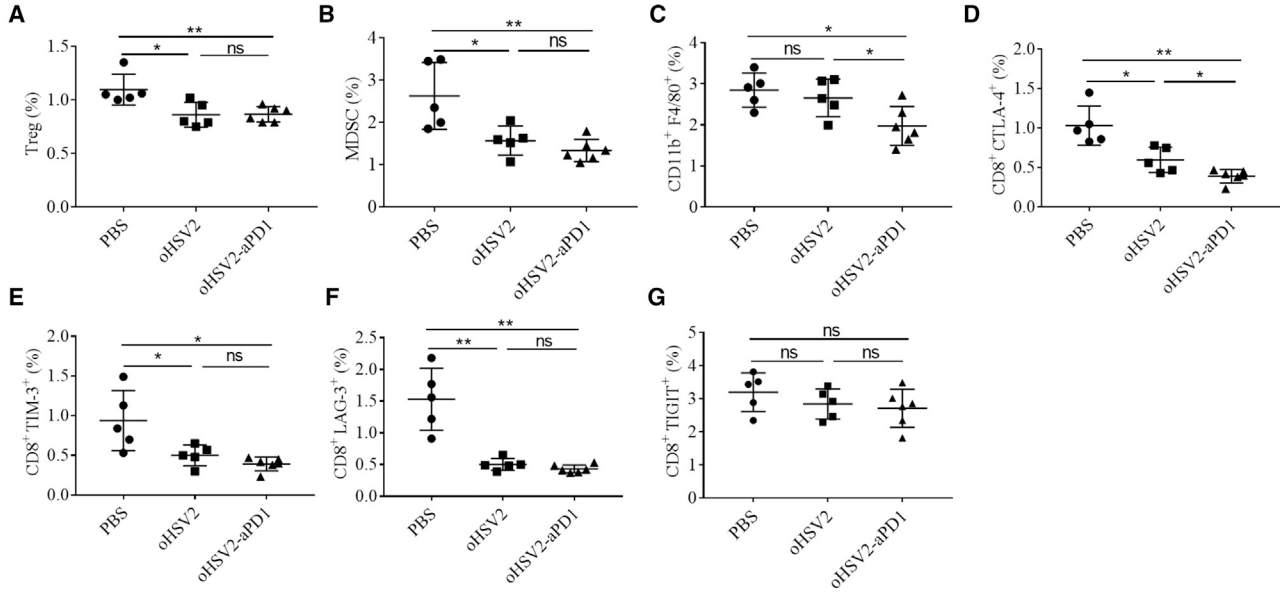

Figure 5. oHSV2-aPD1 Therapy Reduces Inhibitory Immune Cells in the Spleen

C57BL/6J-Pdcd1 mice were subcutaneously inoculated with 2×10^5 B16R and treated as described in the Materials and Methods. Tumor-bearing mice were euthanized 5 days after the last treatment. (A–G) Spleens were collected and analyzed to determine levels of Tregs (defined as $CD4^+CD25^+FoxP3^+$) (A), MDSCs (defined as $CD45^{+-}CD11b^+Gr\text{-}1^+$) (B), $CD45^+CD11b^+F4/80^+$ (C), and $CD8^+$ T cell exhaustion (D–G). Data are presented as individual replicates. *p < 0.05, **p < 0.01. ns, not significant.

cell adhesion and migration, cytokines and receptors, chemokines and receptors, interferon response, TNF superfamily, and the complement pathway. $CD4^+$ T cells, $CD8^+$ T cells, Th1 cells, neutrophils, cytotoxic cells, and memory T cells were also elevated in the oHSV2-aPD1-treated group compared with the isotype-treated group. A similar phenomenon was also observed in spleen tissues (Figure 7B), and these results were consistent with those of the previous analysis of splenic cells using flow cytometry.

Taken together, these data indicate that local administration of oHSV2-aPD1 induces the most significant activation of immune effectors in both the TME and the systemic immune system compared with mono-therapies (local application of oHSV2 or systemic application of anti-PD1).

DISCUSSION

At present, tumors are a significant threat to human health and longevity worldwide. Although the classical therapies, including surgery, chemotherapy, radiation, and targeting drugs, have made great achievements, treatment effects are not always satisfactory, especially in advanced tumors. Recently, immunotherapies, represented by ICBs, have gained increasing attention as an attractive strategy for cancer treatment. In October 2018, James Allison and Tasuku Honjo shared the Nobel Prize in Physiology or Medicine for their contributions to CTLA-4 and PD-1 therapies.[29]

In the present study, we report on a novel OV, oHSV2-aPD1, in which the oHSV2 virus is engineered to express an anti-hPD1mAb to provide a combinatorial immunotherapy strategy. Here, we found that oHSV2-aPD1-infected eukaryotic cells produced and secreted anti-hPD1mAb. The ability of the mAb to bind human PD-1 was confirmed by western blotting. Biological functionality was confirmed in PBMCs from cancer patients. Through virus infection experiments and Cell Counting Kit-8 (CCK8) cell viability assays, we observed that the introduction of the anti-hPD1mAb sequence into the viral backbone did not alter the oncolytic spectrum, nor did it hinder the cytolytic activity of oHSV2-aPD1. In the B16R melanoma model, representing an immunosuppressive tumor, oHSV2-aPD1 effectively delayed tumor progression and induced a durable antitumor response.

PD-1, a negative regulator of the pre-existing immune response, is typically expressed on the surface of activated T cells. Once PD-1 is engaged by PD-L1, which is mainly expressed on tumor cells as well as lymphocytes, it can induce T cell exhaustion.[30] Compared with oHSV2, oHSV2-aPD1 has an enhanced oncolytic activity *in vitro* when infecting some cell lines at a medium MOI (MOI = 1), although the expressed anti-hPD1mAb lacks action routes (Figure 2B; Figure S3). It may simply attribute to the high concentration of immunoglobulin in culture supernatants. When at a high MOI, the expression of immunoglobulin was impaired for most tumor cells that were quickly lysed, and when the MOI = 0.1, the immunoglobulin concentration was also quite low for the cells that were infected slowly. *In vivo*, oHSV2-aPD1 has a similar antitumor activity with oHSV2 in the normal mouse melanoma model and an enhanced antitumor effect in the C57BL/6J-Pdcd1 mouse model. This was mainly attributed to that the anti-hPD1mAb encoded by oHSV2-aPD1 bound and neutralized the humanized PD-1 expressed on the T cells of

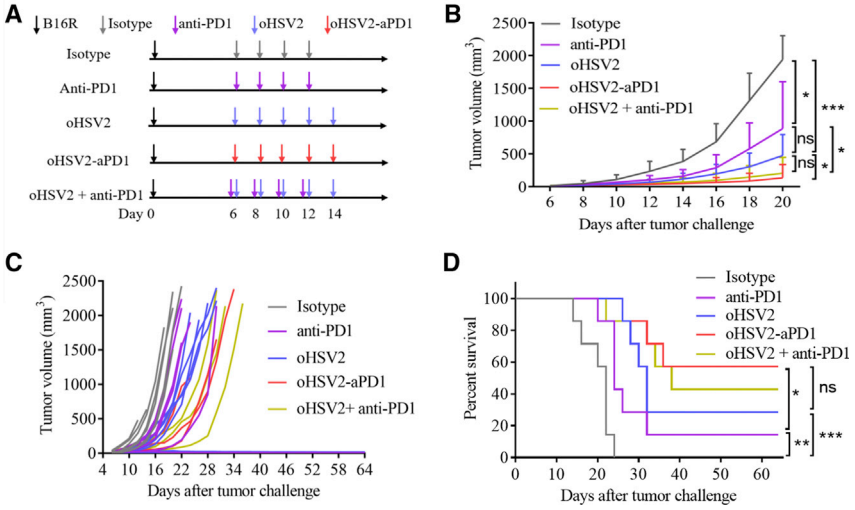

Figure 6. Combination of oHSV2 and PD-1 Blockade Synergistically Improves Antitumoral Efficacy

C57BL/6J-Pdcd1 mice were subcutaneously inoculated with B16R and treated via intratumoral injection of OVs and/or intraperitoneal injection of antibodies as described in the Materials and Methods (n = 7 per group). (A) Schematic of the experimental design. (B) Tumor volumes were measured every 2 days. Data are presented as the mean + SD. (C) Tumor volumes for each mouse are shown separately. (D) Survival is monitored by Kaplan-Meier analysis, and statistical analyses were performed using log rank test. *p < 0.05, **p < 0.01, ***p < 0.001. ns, not significant.

transgenic mouse. Although the initial treatment dosage of viruses was about MOI = 1, as the tumors grew or decreased, the following relative dosages were much lower or higher than MOI = 1. Thus, it is a comprehensive dose effect *in vivo*.

A clinical trial testing pembrolizumab in patients with metastatic melanoma demonstrated that the pre-existing $CD8^+$ T cells located around the invasive tumor correlated with the expression of PD-1/PD-L1. Further, this $CD8^+$ T cell population was more meaningful than PD-L1 expression in predicting treatment responses.[11] However, many cancers display a limited T cell infiltration, mostly because of a microenvironment with few neoantigens and, thus, low immunogenicity.[31] These barriers seem to be overcome by the use of OVs. By selectively lysing neoplastic cells resulting in immunogenic cancer cell death (ICD), OVs could cause the release of TAAs, danger-associated molecular patterns (DAMPs), and pathogen-associated molecular patterns (PAMPs), thus creating a pro-immune cytokine environment that promotes antigen presentation, recruits T cells, and leads to priming of tumor-specific T cells.[32] OVs can also facilitate T cell infiltration through the induction of potent type I interferon responses, which increase the production of chemokines.[33] Similarly, our study demonstrated that, compared with the isotype and anti-PD1 groups, both virus groups significantly activated Th1, neutrophils, DCs, MHC class I and II, adhesion molecules, chemokines, cytokines, interferons, complement pathway members, and TNF superfamily members in tumors (Figure 7B). Together, these activated components led to a significant infiltration of T cells in the TME, thus promoting the antitumor activity of OV themselves and enhancing the therapeutic effects of ICB.

To acquire a more significant and durable antitumor response, many strategies had been developed to combine ICB with various types of OVs. Gao et al.[34] found that targeted recombinant vesicular stomatitis virus (VSV) combined with anti-CTLA-4 mAb was more effective than either treatment alone. Another study reported that combined localized Newcastle disease virus (NDV) and systemic CTLA-4 blockade treatment resulted in rejection of pre-established distant tumors (no injection of virus) and resistance to a second challenge in B16 melanoma models.[35] Dias et al.[25] generated an oncolytic adenovirus expressing full-length human CTLA-4 mAb and found that local administration resulted in 43-fold higher anti-CTLA-4 mAb concentrations in the tumor versus plasma. Kleinpeter et al.[36] reported an oncolytic vaccinia virus (WR-mAb) expressing a monoclonal IgG (named J43) against the murine PD-1. This study found that the tumoral mAb concentration was higher and lasted longer upon intratumoral administration of WR-mAb versus 10 μg intratumoral injection of J43. However, WR-mAb did not improve antitumor activity in B16F10 compared with the parental, unarmed WR.[36] Recently, a team led by Passaro[37] modified an oncolytic HSV1 to express a single-chain PD-1 antibody, and found that this system induced a durable therapeutic effect in two mouse glioblastoma models. However, the durable antitumor response may not be applicable to all OVs, because attenuated measles virus (MV) vectors expressing antibodies against marine CTLA-4 or PD-L1 delayed tumor progression and prolonged survival but did not achieve durable therapeutic benefits in a B16 murine model.[38] In this study, we have engineered the first oHSV2 armed with a full mAb against human PD-1. In the poorly immunogenic humanized-PD-1 B16R melanoma mouse model, oHSV2-aPD1 led to a distinct reduction in tumor burden and an increase in survival (Figures 3B–3D). The antitumor response was as effective as the combination of local application of unarmed oHSV2 with systemic administration of anti-PD1 and was superior to either treatment alone (Figures 6B–6D), suggesting that local delivery of PD-1 inhibitors efficiently promotes OV-induced antitumor response. In addition, intratumoral injection of oHSV2-aPD1 induced an immune memory that protected hosts against further melanoma challenge. This can be attributed to the enhancement of central memory T cells (Tcms) in the TME and the systemic immune system (Figure 7B). Tems (Figure 7B) were also increased in the spleen of oHSV2-aPD1-treated mice, as confirmed by measurement of $CD44^+$ memory T cells compared with controls (Figures 4E and 4F).

Local administration of oHSV2-aPD1 elicited pronounced changes in systemic immunity. RNA sequencing analysis revealed that, relative

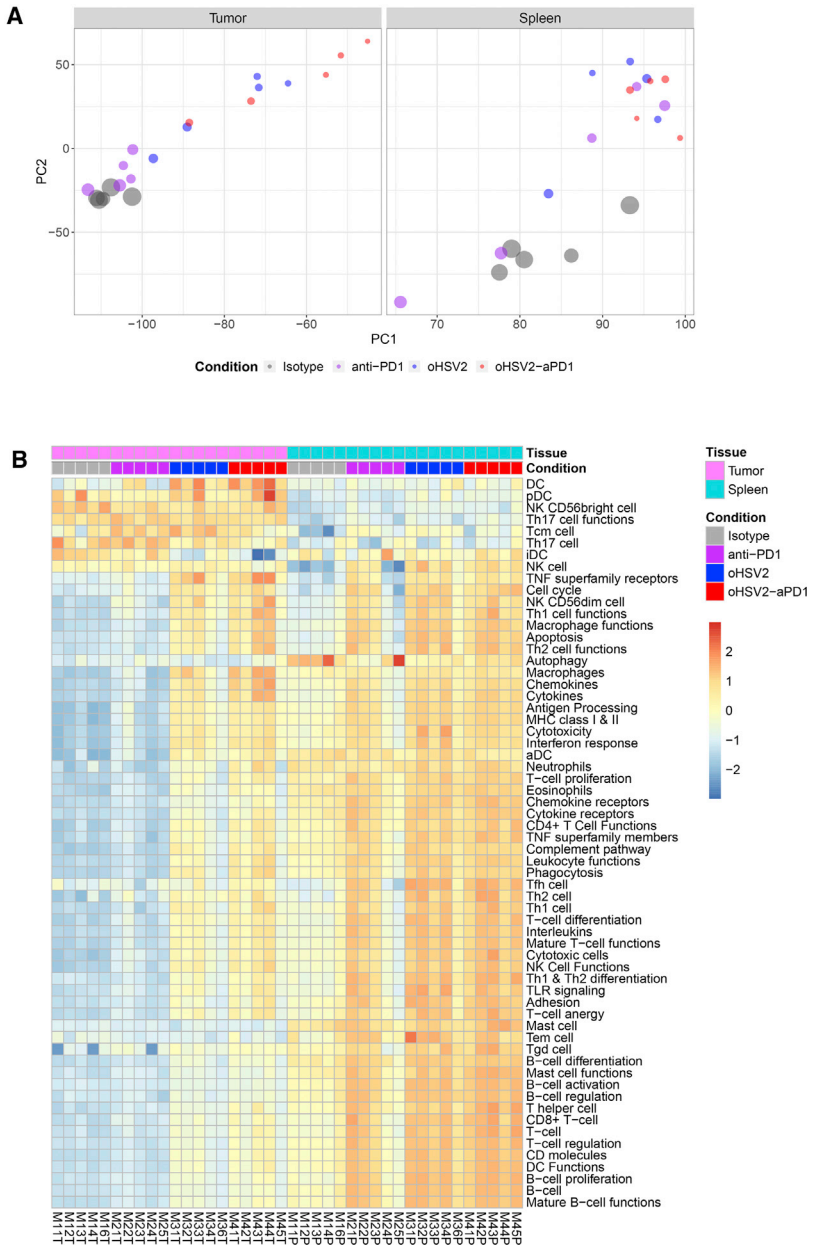

Figure 7. Treatment with oHSV2-aPD1 Induces Activation of Immune Effectors in Tumor and Spleen Tissues

(A) PCA plot showing gene expression in tumor (left circles) and spleen (right circles) tissues. The areas of the circles represent tumor volumes at the time of specimen collection. (B) Heatmap of the immune profile in tumor (left) and spleen (right) tissues. Rows represent the immune features, and columns represent individual specimens. Unsupervised clustering algorithm (UCA) was conducted to cluster immune features based on similar expression patterns.

to the control, many immune effector cells and molecules, such as B cells, $CD4^+$ T cells, $CD8^+$ T cells, Th1, DCs, cytotoxic cells, chemokines, interferons, TNF superfamily members, and complement pathway members, were activated in spleens from oHSV2-aPD1-treated animals (Figure 7B). Flow cytometry analysis of splenic cells also confirmed an enhancement in the proportion of $CD4^+$ T cells, $CD3^+$ T cells, $CD8^+$ T cells, DCs, and $CD8^+$ T cells coexpressing ICOS, IL-2, IFN-γ, TNF-α, and Ki67 following oHSV2-aPD1 treatment (Figures 4A–4C and 4G–4L). This was consistent with a report by Chen et al.,[28] which demonstrated that a combination of oncolytic HSV1 administration and PD-1 blockade induced increased infiltration of $CD3^+/CD4^+/CD8^+$ T cells and memory T cells in the spleen. Woller et al.[39] also found that a combination of oncolytic adenovirus and PD-1 antibody enhanced the breadth and magnitude of antitumor T cells. In addition, we found that oHSV2-aPD1 therapy caused a significant decline in splenic immunosuppressive cells, including Tregs, MDSCs, and $CD11b^+F4/80^+$ cells (Figures 5A–5C). Surprisingly, exhausted $CD8^+$ cells expressing coinhibitory molecules (CTLA-4, TIM-3, and LAG-3) were also diminished following oHSV2-aPD1 treatment (Figures 5D–5F). In summary, through these alterations in the splenic immune profile, oHSV2-aPD1 enhanced systemic antitumor immunity, thus inducing durable antitumor activity and prolonged survival.

Interestingly, RNA sequencing analysis revealed that, compared with tumor tissues, the immune profile of spleen tissues had a better correlation with the therapeutic effect (Figures 7A and 7B). This was particularly apparent in the anti-PD1 treatment group, where the three mice with better response were distinct from the two mice with a more general response. This is likely attributable to the larger population of immune cells in peripheral immune organs compared with the TME, indicating that systemic immunity may play a more important role in the antitumor response compared with local immunity. Thus, detection of the immune effector cells or molecules in the peripheral immune system, including in the peripheral blood, can be a convenient and practical strategy for predicting the efficacy of immunotherapy.

Our study has two limitations. One is oHSV2-aPD1 and oHSV2 treatment do not have a statistical difference in survival times. It might because the malignancy of the B16R melanoma model was too high. Tumors grew quickly, and mouse death occurred 14 (Figures 6B–6D) or 16 days (Figures 3B–3D) after tumor challenge even though the tumor volume just reached 500 mm^3. The other limitation is that the distribution and metabolism of oHSV2-aPD1 and the secreted antibody were not evaluated *in vivo*. In the future, we will further study these aspects, as well as any possible adverse effects.

In conclusion, our findings suggest that oHSV2-aPD1 demonstrates enhanced antitumor activity and exerts a durable response in preclinical melanoma models, indicating that it may be a promising therapeutic agent for clinical translation.

MATERIALS AND METHODS

Cell Lines

The cell lines used in this study included Vero (*Cercopithecus aethiops* kidney epithelial cell), CT26 (mouse colon carcinoma cell), B16F10 (mouse melanoma cell), B16R (mouse melanoma cell), 4T1 (mouse mammary carcinoma cell), A549 (human lung carcinoma cell), BGC823 (human gastric cancer cell), HuH7 (human hepatocarcinoma cell), HT29 (human colorectal adenocarcinoma cell), H1299 (human non-small cell lung cancer cell), SKOV3 (human ovarian adenocarcinoma cell), KMRC3 (human renal clear cell carcinoma cell), BCPAP (human thyroid papillary carcinoma cell), KYSE30 (human esophageal squamous carcinoma cell), CAL27 (human tongue squamous carcinoma cell), FaDu (human pharynx squamous carcinoma cell), U373 (human brain glioma cell), TSU (human prostate cancer cell), and MCF7 (human mammary adenocarcinoma cell). Vero, 4T1, H1299, and KYSE30 were obtained from ATCC and kept in our laboratory. CT26, B16F10, A549, BGC823, HuH7, HT29, SKOV3, CAL27, FaDu, TSU, and MCF7 were obtained from the Cell Resource Center, Peking Union Medical College. KMRC3, BCPAP, and U373 were maintained in our laboratory. B16R, stably transfected with an HSV receptor, was constructed in our laboratory.[26] Vero, B16F10, B16R, 4T1, BGC823, HuH7, HT29, SKOV3, CAL27, FaDu, TSU, and MCF7 were cultured in DME/F-12 medium supplemented with 10% fetal bovine serum (FBS). CT26, A549, H1299, KMRC3, BCPAP, KYSE30, and U373 were cultured in RPMI-1640 medium supplemented with 10% FBS. All cell lines above were grown in a 37°C, 5% CO_2 incubator.

Mice

Six-week-old female transgenic C57BL/6J-Pdcd1 mice, which had a humanized PD-1, were obtained from Shanghai Model Organisms Center (Shanghai, China). Six-week-old female normal C57BL/6J mice were purchased from Beijing Vital River Laboratory Animal Technology Company (Beijing, China). All animals were housed in specific pathogen-free (SPF) conditions. All animal experiments were approved by the Experimental Animal Committee of the Cancer Hospital, Chinese Academy of Medical Sciences.

Plasmid Construction

Several plasmids were constructed to insert the anti-hPD1mAb sequences into oHSV2 genome. First, we constructed a shuttle plasmid pHG52d34.5-CMV-eGFP based on pHG52d34.5 plasmid,[23] which contains the upstream and downstream (DS) flanking regions (FLRs) of ICP34.5 gene. The CMV-eGFP cassette was derived from pcDNA3.1-CMV-eGFP plasmid and was inserted into the pHG52d34.5 locus between upstream and DS FLRs to get pHG52d34.5-CMV-eGFP.

The anti-hPD1mAb sequences (BMS-936558) were disclosed in the database IMGT (http://www.imgt.org/3Dstructure-DB/cgi/details.cgi?pdbcode = 9623). Both the heavy and light chains were generated a synthetic way (Genewiz, Suzhou, China) with the B cell antigen receptor signal sequence. To construct the pHG52d34.5-DC-aPD1 plasmid, we inserted the heavy chain and light chain into the pHG52d34.5-DC orderly, which had a CMV promotor and an RSV-LTR promotor between the upstream and DS FLRs of ICP34.5. Both the shuttle plasmids pHG52d34.5-CMV-eGFP and pHG52d34.5-DC-aPD1 were cloned by standard cloning techniques and verified by sequencing after construction completion.

Virus Construction

oHSV2-aPD1 was engineered from oHSV2, which is derived from the HG52 strain as previously described.[23] The pHG52d34.5-CMV-eGFP and pHG52d34.5-DC-aPD1 transfer vectors were used to construct oHSV2-aPD1 through two rounds of homologous recombination. In brief, the shuttle plasmid pHG52d34.5-CMV-eGFP was inserted into the ICP34.5 locus of oHSV2 by cotransfection into Vero cells. The recombined vector oHSV2-eGFP was purified with six rounds of plaque assays by a fluorescent microscope. Next, the pHG52d34.5-DC-aPD1 shuttle plasmid was used to replace the CMV-eGFP gene by a similar procedure, resulting in the oHSV2-aPD1 virus. The final recombinant oHSV2-aPD1 and oHSV2 stocks were amplified in Vero cells, titrated, divided into aliquots, and stored at −80°C until usage.

DNA Ladder Analysis

Vero cells were infected with viruses at MOI = 0.1. After 48 h, the infected cells were gathered and lysed in DNAzol (DP3001; BioTeke Corporation, China). Then DNA was collected and washed by 75% ethanol. After PCR amplification using the primers from the anti-hPD1mAb light chain or heavy chain, DNA ladders were analyzed by 1% agarose gel electrophoresis.

Western Blotting Analysis

Vero, A549, CT26, or B16R cells were infected with oHSV2-aPD1 at MOI = 0.1. After 48 h, cell culture supernatants were filtered by 0.45-μm filters and purified with protein G agarose (TransGen, Beijing, China). Next, 25 μL of purified antibodies was prepared in loading buffer and loaded onto a 5%–12% polyacrylamide gel. Proteins were then transferred onto a polyvinylidene fluoride (PVDF) membrane or directly stained with Coomassie brilliant blue. Membranes were saturated at room temperature in blocking buffer and incubated with HRP-conjugated goat anti-human IgG (H+L) antibody (A18811; Invitrogen) overnight at 4°C. Signal detection was performed by Super ECL Plus western blotting detection reagents (ApplyGen, Beijing, China).

For the analysis of binding ability of the expressed anti-hPD1mAb, human PD-1 protein (His-tag) (10377-H08H; Sino Biological Incorporation, Beijing, China) and a His-tagged protein (a gift from Prof. Qun Wei, Beijing Normal University, China) were run on a 5%–12% polyacrylamide gel. The membrane with transferred protein was incubated with the purified anti-hPD1mAb expressed by oHSV2-aPD1-infected CT26 cells, washed, and incubated with a secondary

antibody HRP-conjugated goat anti-human IgG (H+L) (A18811; Invitrogen).

Anti-hPD1mAb Biological Activity *In Vitro*

Six-milliliter peripheral blood samples were prepared with EDTA-K2 tubes, and PBMCs were isolated by centrifugation through a Histopaque density gradient (H8889; Sigma). Next, PBMCs were stimulated with culture supernatants of oHSV2 or oHSV2-aPD1-infected or mock-infected A549 cells (filtered by 0.22-μm filters), 1 μg/mL ionomycin (BioGems, USA), and 50 ng/mL PMA (BioGems, USA). After being cultured in a 37°C, 5% CO_2 incubator for 36 h, supernatants were collected for analysis of IFN-γ and IL-2 levels with human IFN-γ Pre-Coated ELISA Kit (BGK01579; BioGems) and human IL-2 Pre-Coated ELISA Kit (BGK60568; BioGems). Every sample was tested with a duplicate. All PBMCs from patients with advanced tumors were obtained after informed consent, and the collection of human specimens obtained approval from the Ethics Committee of National Cancer Center/Cancer Hospital, Chinese Academy of Medical Sciences and Peking Union Medical College.

Virus Infection Experiment *In Vitro*

For oncolytic spectrum observation, mouse and human tumor cell lines, including B16F10, B16R, CT26, 4T1, A549, H1299, KYSE30, BGC823, BCPAP, HuH7, KMRC3, HT29, SKOV3, CAL27, FaDu, and U373, were seeded in six-well plates at a quantity of 4×10^5 per well, cultured overnight, and then infected with oHSV2 or oHSV2-aPD1 or mock infected at MOI = 1. Photomicrographs were taken 24 h later.

CCK8 Cell Viability Assay

Cell viability was examined by a CCK8 assay using Cell Counting Kit-8 (DOJINDO, Japan). Cells were seeded in 96-well plates at a quantity ranging from 5×10^3 to 1×10^4. Every sample was tested with three duplicates. To test the effect of MOI on cell viability, each cell line was infected 24 h later with oHSV2 or oHSV2-aPD1, or mock infected at MOIs of 0.1, 1, and 5. After 24, 48, and 72 h, the culture medium was discarded and 100 μL of a mixture containing 10% CCK8 was added and incubated for another 2 h. The plates were measured using a model 550 microplate reader (Bio-Rad, Japan) at 450 nm.

Tumor Models

B16R cells (2×10^5/mouse) were inoculated subcutaneously into the right flanks of C57BL/6J-Pdcd1 or C57BL/6J mice. When the average diameter of the tumors reached 5 mm, the mice were given intratumoral or peri-tumoral injection of PBS, oHSV2, or oHSV2-aPD1 at 2×10^5 plaque-forming units (PFUs) per tumor every 2 days for five times in total. In some experiments, mice were euthanized 5 days after the last treatment to collect spleens for cytotoxic activity experiments or flow cytometry analysis. For the comparison of combined therapies and monotherapies, grouped mice were also given intraperitoneal injection of isotype antibody (Purified Human IgG4 Control; 403402; BioLegend) or anti-human PD-1 antibody (Recombinant anti-Human PD-1 Monoclonal Antibody; kx10-1; Beijing Kexin Biotech, China) at 200 μg/mouse every other day for a total of four times. Ten mice treated with anti-PD1, oHSV2, oHSV2-aPD1, or anti-PD1 plus oHSV2, which survived more than 64 days, were rechallenged subcutaneously into left flanks with 2×10^5 B16R cells per mouse, and naive C57BL/6J-Pdcd1 mice received same dose tumor cells as a control. In some experiments, spleens and tumor tissues were collected 5 days after the last treatment for transcriptome sequencing.

Tumor diameter was measured every 2 days using an electric caliper and was used to calculate tumor volume (mm^3) ([major axis; mm] × [minor axis; mm]^2 × 0.52). During the experiments, mice were euthanized when tumor volume reached 2,500 mm^3 to avoid unnecessary suffering. The presentation of tumor volume was stopped when the mouse death occurred or the tumor volume reached 2,500 mm^3.

Cytotoxic Activity Experiment

Splenic lymphocytes, which were isolated by centrifugation in a gradient lymphocyte isolation solution for mice, were seeded on 96-well plates and cocultured with 5- (and 6-) carboxy fluorescein diacetate succinimidyl ester (CFSE) (1820837; Life Technologies) staining B16R cells at a ratio of 25:1, 50:1, or 100:1. After 6 h, supernatants were discarded, and cells were resuspended by propidium iodide (SL7090; Coolaber, Beijing, China) working solutions and analyzed using flow cytometry in 20 min.

Flow Cytometry Analysis

Single cells were isolated from collected spleens by centrifugation in a gradient lymphocyte isolation solution for mice. Next, single-cell suspensions were blocked with CD16/32 antibody (14-0161-85; eBioscience) and then stained with antibodies against mouse CD4 (fluorescein isothiocyanate [FITC], 100509; BioLegend), CD8 (phycoerythrin [PE] or FITC, 100707 or 100705; BioLegend), CD3 (FITC, 100305; BioLegend), NK-1.1 (PE/Cy5, 108715; BioLegend), CD44 (allophycocyanin [APC], 103011; BioLegend), CD45 (PerCP/Cy5.5, 103132; BioLegend), CD11b (PE, 101207; BioLegend), CD11c (FITC, 557400; BD Biosciences), Ly-6G (APC, 127613; BioLegend), CD278 (PE, 117405; BioLegend), CD25 (APC, 17-0251-81; eBioscience), F4/80 (FITC, 11-4801-81; eBioscience), Gr-1 (FITC, 108405; BioLegend), TIGIT (PE/Cy7, 142107; BioLegend), CD152 (PerCP/Cy5.5, 106315; BioLegend), CD366 (PerCP/Cy5.5, 134011; BioLegend), or CD223 (PerCP/Cy5.5, 125211; BioLegend), or intracellularly stained with IL-2 (APC, 503809; BioLegend), IFN-γ (APC, 17-7311-81; eBioscience), TNF-α (APC, 17-7321-81; eBioscience), Ki-67 (PE, 652404; BioLegend), or Foxp3 (PE, 12-4771-80; eBioscience) following the instructions of the Foxp3/Transcription Factor Staining Buffer Set (00-5523-00; eBioscience). Samples were collected on BD LSR II, and data were analyzed using FlowJo software.

RNA Sequencing Analysis

Corresponding tumor and spleen tissues were surgically removed from mice 5 days after the last treatment and preserved in 2 mL RNAlater (AM7021; Invitrogen) immediately. Total RNA was extracted with a TRIzol reagent (15596018; Ambion), then was used to prepare

the eukaryotic strand-specific library and sequenced by an Illumina Hiseq-PE150.The data were normalized and analyzed with the "DESeq2" R package.

Statistics

Unless otherwise stated, quantitative data are presented as the mean ± SD. Statistical analyses were performed using GraphPad Prism software (version 7.00; San Diego, CA, USA). ELISA, flow cytometry, CCK8, and tumor volumes data were analyzed by Tukey's multiple comparison test and an ANOVA. Animal survival was presented using Kaplan-Meier survival curves and statistically analyzed by log rank (Mantel-Cox) test. Two-sided $p < 0.05$ was considered statistically significant: *$p < 0.05$; **$p < 0.01$; ***$p < 0.001$; ****$p < 0.0001$; ns, not significant.

SUPPLEMENTAL INFORMATION

Supplemental Information can be found online at https://doi.org/10.1016/j.omto.2019.10.003.

AUTHOR CONTRIBUTIONS

Y.Z., X.H., Z.Y., L.Z., and X.D. performed the experiments. W.Z., K.Z., and B.L. designed the experiments. Y.Z., W.Z, X.H., and L.F. analyzed the data. Y.Z. wrote the paper. B.L., K.Z., W.Z., S.C., and L.F. made suggestions for the manuscript.

CONFLICTS OF INTEREST

The authors declare no competing interests.

ACKNOWLEDGMENTS

This research was supported by a grant from Chinese Academy of Medical Sciences Initiative for Innovative Medicine (2016-I2M-1-001) and a grant from National Major Scientific and Technological Special Project for "Significant New Drugs Development" during the Thirteenth Five-year Plan Period (2018ZX09733002).

REFERENCES

1. Weber, J., Thompson, J.A., Hamid, O., Minor, D., Amin, A., Ron, I., Ridolfi, R., Assi, H., Maraveyas, A., Berman, D., et al. (2009). A randomized, double-blind, placebo-controlled, phase II study comparing the tolerability and efficacy of ipilimumab administered with or without prophylactic budesonide in patients with unresectable stage III or IV melanoma. Clin. Cancer Res. *15*, 5591–5598.

2. Brahmer, J.R., Tykodi, S.S., Chow, L.Q.M., Hwu, W.-J., Topalian, S.L., Hwu, P., Drake, C.G., Camacho, L.H., Kauh, J., Odunsi, K., et al. (2012). Safety and activity of anti-PD-L1 antibody in patients with advanced cancer. N. Engl. J. Med. *366*, 2455–2465.

3. Petrylak, D.P., Powles, T., Bellmunt, J., Braiteh, F., Loriot, Y., Morales-Barrera, R., Burris, H.A., Kim, J.W., Ding, B., Kaiser, C., et al. (2018). Atezolizumab (MPDL3280A) monotherapy for patients with metastatic urothelial cancer: long-term outcomes from a phase 1 study. JAMA Oncol. *4*, 537–544.

4. Gettinger, S.N., Horn, L., Gandhi, L., Spigel, D.R., Antonia, S.J., Rizvi, N.A., Powderly, J.D., Heist, R.S., Carvajal, R.D., Jackman, D.M., et al. (2015). Overall survival and long-term safety of nivolumab (anti-programmed death 1 antibody, BMS-936558, ONO-4538) in patients with previously treated advanced non-small-cell lung cancer. J. Clin. Oncol. *33*, 2004–2012.

5. Sanmamed, M.F., and Chen, L. (2018). A Paradigm Shift in Cancer Immunotherapy: From Enhancement to Normalization. Cell *175*, 313–326.

6. Le, D.T., Durham, J.N., Smith, K.N., Wang, H., Bartlett, B.R., Aulakh, L.K., Lu, S., Kemberling, H., Wilt, C., Luber, B.S., et al. (2017). Mismatch repair deficiency predicts response of solid tumors to PD-1 blockade. Science *357*, 409–413.

7. Postow, M.A., Chesney, J., Pavlick, A.C., Robert, C., Grossmann, K., McDermott, D., Linette, G.P., Meyer, N., Giguere, J.K., Agarwala, S.S., et al. (2015). Nivolumab and ipilimumab versus ipilimumab in untreated melanoma. N. Engl. J. Med. *372*, 2006–2017.

8. Robert, C., Schachter, J., Long, G.V., Arance, A., Grob, J.J., Mortier, L., Daud, A., Carlino, M.S., McNeil, C., Lotem, M., et al.; KEYNOTE-006 investigators (2015). Pembrolizumab versus Ipilimumab in Advanced Melanoma. N. Engl. J. Med. *372*, 2521–2532.

9. Rizvi, N.A., Hellmann, M.D., Snyder, A., Kvistborg, P., Makarov, V., Havel, J.J., Lee, W., Yuan, J., Wong, P., Ho, T.S., et al. (2015). Cancer immunology. Mutational landscape determines sensitivity to PD-1 blockade in non-small cell lung cancer. Science *348*, 124–128.

10. Garon, E.B., Rizvi, N.A., Hui, R., Leighl, N., Balmanoukian, A.S., Eder, J.P., Patnaik, A., Aggarwal, C., Gubens, M., Horn, L., et al.; KEYNOTE-001 Investigators (2015). Pembrolizumab for the treatment of non-small-cell lung cancer. N. Engl. J. Med. *372*, 2018–2028.

11. Tumeh, P.C., Harview, C.L., Yearley, J.H., Shintaku, I.P., Taylor, E.J.M., Robert, L., Chmielowski, B., Spasic, M., Henry, G., Ciobanu, V., et al. (2014). PD-1 blockade induces responses by inhibiting adaptive immune resistance. Nature *515*, 568–571.

12. Kaufman, H.L., Kohlhapp, F.J., and Zloza, A. (2015). Oncolytic viruses: a new class of immunotherapy drugs. Nat. Rev. Drug Discov. *14*, 642–662.

13. Mell, L.K., Brumund, K.T., Daniels, G.A., Advani, S.J., Zakeri, K., Wright, M.E., Onyeama, S.-J., Weisman, R.A., Sanghvi, P.R., Martin, P.J., and Szalay, A.A. (2017). Phase I trial of intravenous oncolytic vaccinia virus (GL-ONC1) with cisplatin and radiotherapy in patients with locoregionally advanced head and neck carcinoma. Clin. Cancer Res. *23*, 5696–5702.

14. Geletneky, K., Hajda, J., Angelova, A.L., Leuchs, B., Capper, D., Bartsch, A.J., Neumann, J.-O., Schöning, T., Hüsing, J., Beelte, B., et al. (2017). Oncolytic H-1 Parvovirus Shows Safety and Signs of Immunogenic Activity in a First Phase I/IIa Glioblastoma Trial. Mol. Ther. *25*, 2620–2634.

15. Kaufman, H.L., Andtbacka, R.H.I., Collichio, F.A., Wolf, M., Zhao, Z., Shilkrut, M., Puzanov, I., and Ross, M. (2017). Durable response rate as an endpoint in cancer immunotherapy: insights from oncolytic virus clinical trials. J. Immunother. Cancer *5*, 72.

16. Garcia-Carbonero, R., Salazar, R., Duran, I., Osman-Garcia, I., Paz-Ares, L., Bozada, J.M., Boni, V., Blanc, C., Seymour, L., Beadle, J., et al. (2017). Phase 1 study of intravenous administration of the chimeric adenovirus enadenotucirev in patients undergoing primary tumor resection. J. Immunother. Cancer *5*, 71.

17. Liu, Z., Ravindranathan, R., Kalinski, P., Guo, Z.S., and Bartlett, D.L. (2017). Rational combination of oncolytic vaccinia virus and PD-L1 blockade works synergistically to enhance therapeutic efficacy Zuqiang. Nat. Commun. *8*, 14754.

18. Bourgeois-Daigneault, M.-C., Roy, D.G., Aitken, A.S., El Sayes, N., Martin, N.T., Varette, O., Falls, T., St-Germain, L.E., Pelin, A., Lichty, B.D., et al. (2018). Neoadjuvant oncolytic virotherapy before surgery sensitizes triple-negative breast cancer to immune checkpoint therapy. Sci. Transl. Med. *10*, eaao1641.

19. Samson, A., Scott, K.J., Taggart, D., West, E.J., Wilson, E., Nuovo, G.J., Thomson, S., Corns, R., Mathew, R.K., Fuller, M.J., et al. (2018). Intravenous delivery of oncolytic reovirus to brain tumor patients immunologically primes for subsequent checkpoint blockade. Sci. Transl. Med. *10*, eaam7577.

20. Moesta, A.K., Cooke, K., Piasecki, J., Mitchell, P., Rottman, J.B., Fitzgerald, K., Zhan, J., Yang, B., Le, T., Belmontes, B., et al. (2017). Local delivery of OncoVEXmGM-CSF generates systemic antitumor immune responses enhanced by cytotoxic T-lymphocyte-associated protein blockade. Clin. Cancer Res. *23*, 6190–6202.

21. Ribas, A., Dummer, R., Puzanov, I., VanderWalde, A., Andtbacka, R.H.I., Michielin, O., Olszanski, A.J., Malvehy, J., Cebon, J., Fernandez, E., et al. (2017). Oncolytic Virotherapy Promotes Intratumoral T Cell Infiltration and Improves Anti-PD-1 Immunotherapy. Cell *170*, 1109–1119.e10.

22. Gujar, S., Pol, J.G., and Kroemer, G. (2018). Heating it up: Oncolytic viruses make tumors 'hot' and suitable for checkpoint blockade immunotherapies. OncoImmunology *7*, e1442169.

23. Zhao, Q., Zhang, W., Ning, Z., Zhuang, X., Lu, H., Liang, J., Li, J., Zhang, Y., Dong, Y., Zhang, Y., et al. (2014). A novel oncolytic herpes simplex virus type 2 has potent anti-tumor activity. PLoS ONE *9*, e93103.

24. Colgrove, R., Diaz, F., Newman, R., Saif, S., Shea, T., Young, S., Henn, M., and Knipe, D.M. (2014). Genomic sequences of a low passage herpes simplex virus 2 clinical isolate and its plaque-purified derivative strain. Virology *450–451*, 140–145.

25. Dias, J.D., Hemminki, O., Diaconu, I., Hirvinen, M., Bonetti, A., Guse, K., Escutenaire, S., Kanerva, A., Pesonen, S., Löskog, A., et al. (2012). Targeted cancer immunotherapy with oncolytic adenovirus coding for a fully human monoclonal antibody specific for CTLA-4. Gene Ther. *19*, 988–998.

26. Zhuang, X.F., Zhou, A.P., Shi, G.L., Han, X.P., Li, J., Zhang, Y., Zhang, Y.H., Zhang, S.R., and Liu, B.L. (2012). [Generation of a herpes simplex virus-permissive mouse melanoma cell line B16RHSV]. Zhonghua Zhong Liu Za Zhi *34*, 187–191.

27. Twumasi-Boateng, K., Pettigrew, J.L., Kwok, Y.Y.E., Bell, J.C., and Nelson, B.H. (2018). Oncolytic viruses as engineering platforms for combination immunotherapy. Nat. Rev. Cancer *19*, 419–432.

28. Chen, C.Y., Wang, P.Y., Hutzen, B., Sprague, L., Swain, H.M., Love, J.K., Stanek, J.R., Boon, L., Conner, J., and Cripe, T.P. (2017). Cooperation of Oncolytic Herpes Virotherapy and PD-1 Blockade in Murine Rhabdomyosarcoma Models. Sci. Rep. *7*, 2396.

29. Sent, C. (2018). Two Win Nobel for Immune Regulation Discoveries. Cancer Discov. *8*, 1338–1339.

30. Ribas, A., and Wolchok, J.D. (2018). Cancer immunotherapy using checkpoint blockade. Science *359*, 1350–1355.

31. Schumacher, T.N., and Schreiber, R.D. (2015). Neoantigens in cancer immunotherapy. Science *348*, 69–74.

32. Guo, Z.S., Liu, Z., and Bartlett, D.L. (2014). Oncolytic Immunotherapy: Dying the Right Way is a Key to Eliciting Potent Antitumor Immunity. Front. Oncol. *4*, 74.

33. Brown, M.C., Holl, E.K., Boczkowski, D., Dobrikova, E., Mosaheb, M., Chandramohan, V., Bigner, D.D., Gromeier, M., and Nair, S.K. (2017). Cancer immunotherapy with recombinant poliovirus induces IFN-dominant activation of dendritic cells and tumor antigen-specific CTLs. Sci. Transl. Med. *9*, eaan4220.

34. Gao, Y., Whitaker-Dowling, P., Griffin, J.A., Barmada, M.A., and Bergman, I. (2009). Recombinant vesicular stomatitis virus targeted to Her2/neu combined with anti-CTLA4 antibody eliminates implanted mammary tumors. Cancer Gene Ther. *16*, 44–52.

35. Zamarin, D., Holmgaard, R.B., Subudhi, S.K., Park, J.S., Mansour, M., Palese, P., Merghoub, T., Wolchok, J.D., and Allison, J.P. (2014). Localized oncolytic virotherapy overcomes systemic tumor resistance to immune checkpoint blockade immunotherapy. Sci. Transl. Med. *6*, 226ra32.

36. Kleinpeter, P., Fend, L., Thioudellet, C., Geist, M., Sfrontato, N., Koerper, V., Fahrner, C., Schmitt, D., Gantzer, M., Remy-Ziller, C., et al. (2016). Vectorization in an oncolytic vaccinia virus of an antibody, a Fab and a scFv against programmed cell death -1 (PD-1) allows their intratumoral delivery and an improved tumor-growth inhibition. OncoImmunology *5*, e1220467.

37. Passaro, C., Alayo, Q., DeLaura, I., McNulty, J., Grauwet, K., Ito, H., Bhaskaran, V., Mineo, M., Lawler, S.E., Shah, K., et al. (2019). Arming an oncolytic herpes simplex virus Type 1 with a single-chain fragment variable antibody against PD-1 for experimental glioblastoma therapy. Clin. Cancer Res *25*, 290–299.

38. Engeland, C.E., Grossardt, C., Veinalde, R., Bossow, S., Lutz, D., Kaufmann, J.K., Shevchenko, I., Umansky, V., Nettelbeck, D.M., Weichert, W., et al. (2014). CTLA-4 and PD-L1 checkpoint blockade enhances oncolytic measles virus therapy. Mol. Ther. *22*, 1949–1959.

39. Woller, N., Gürlevik, E., Fleischmann-Mundt, B., Schumacher, A., Knocke, S., Kloos, A.M., Saborowski, M., Geffers, R., Manns, M.P., Wirth, T.C., et al. (2015). Viral Infection of Tumors Overcomes Resistance to PD-1-immunotherapy by Broadening Neoantigenome-directed T-cell Responses. Mol. Ther. *23*, 1630–1640.

OMTO, Volume *15*

Supplemental Information

Enhanced Therapeutic Efficacy of a Novel Oncolytic Herpes Simplex Virus Type 2 Encoding an Antibody Against Programmed Cell Death 1

Yujie Zhu, Xiao Hu, Lin Feng, Zhenrong Yang, Lulin Zhou, Xinchun Duan, Shujun Cheng, Wen Zhang, Binlei Liu, and Kaitai Zhang

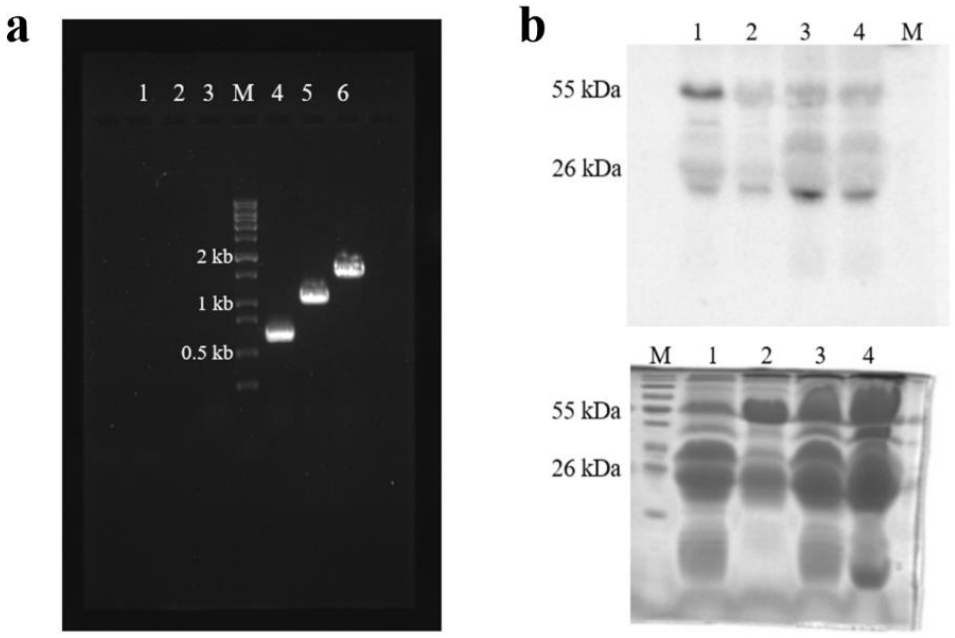

Figure Supplemental 1. The anti-hPD1mAb encoding sequence was inserted and translated correctly

(a) DNA ladder analysis of the modified oHSV2-aPD1 sequences. Lane 1: water light chain (blank control), lane 2: water heavy chain (blank control), lane 3: oHSV2 light chain (negative control), lane 4: oHSV2 heavy chain (negative control), lane 5: oHSV2-aPD1 light chain, lane 6: oHSV2-aPD1 heavy chain. M: molecular marker. **(b)** Culture supernatants from oHSV2-aPD1-infected Vero (lanes 1), A549 (lane 2), CT26 (lane 3) or B16R (lane 4) cells were collected, purified using protein G agarose, and then loaded on SDS-PAGE gels under denaturing conditions. Upper panel: picture following transfer onto PVDF membrane. Lower panel: matched picture of the gel stained with Coomassie brilliant blue. M: molecular marker.

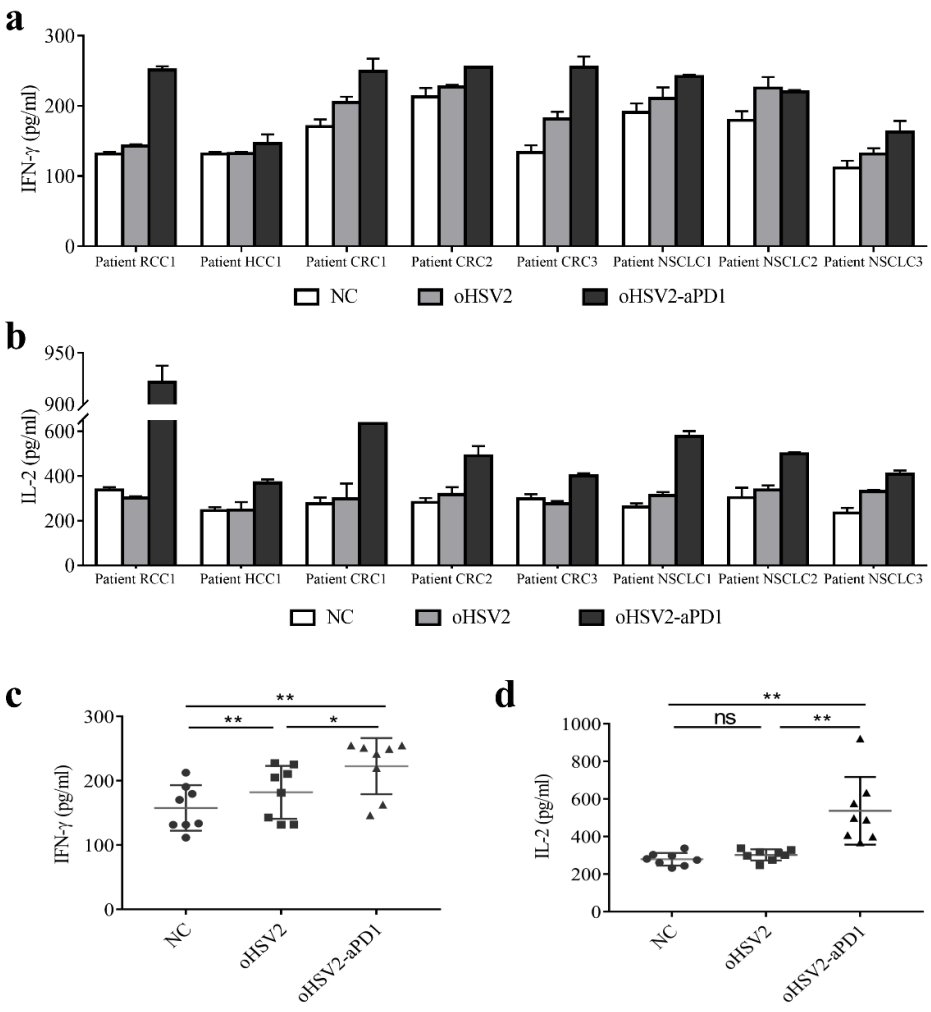

Figure Supplemental 2. Production of IFN-γ and IL-2 in anti-hPD1mAb-stimulated PBMCs from cancer patients

PBMCs from eight advanced tumor patients were treated with filtered culture supernatants from mock-infected (NC, negative control) or OV-infected cells and stimulated with ionomycin and phorbol myristate acetat (PMA). After 36 hours, supernatants were harvested to measure the production of IFN-γ and IL-2 by ELISA. IFN-γ levels **(a)** and IL-2 **(b)** levels in cancer patient PBMCs, with each specimen presented individually. IFN-γ levels **(c)** and IL-2 levels **(d)** in cancer patient PBMCs are shown as statistical results. RCC: renal cell carcinoma, HCC: hepatocellular carcinoma, CRC: colorectal cancer, NSCLC: nonsmall cell lung cancer. Data are presented as the mean ± SD. (*$p < 0.05$; **$p < 0.01$; ns, not significant)

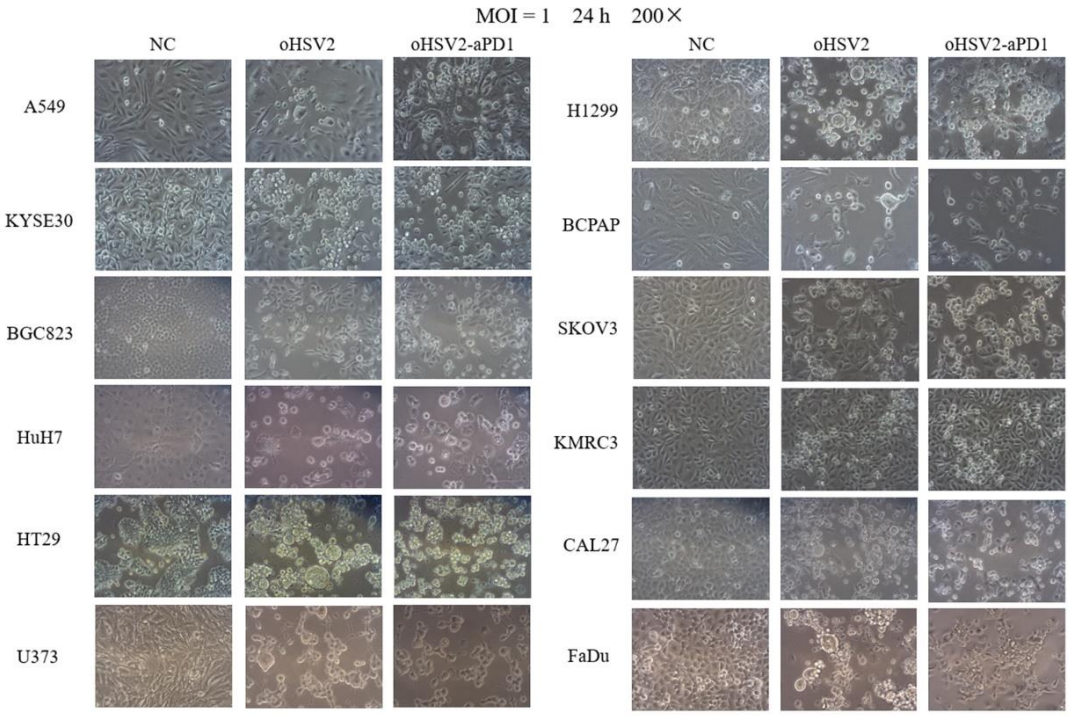

Figure Supplemental 3. Comparison of infectious activities of oHSV2 and oHSV2-aPD1 viruses in human tumor cells

oHSV2 or oHSV2-aPD1 were used to mock-infect or infect human tumor cells, including A549, KYSE30, BGC823, HuH7, HT29, U373, H1299, BCPAP, SKOV3, KMRC3, CAL27 and FaDu cells, at MOI = 1 for 24 hours. Images were collected at 20× objective magnification with an inverted phase contrast microscope.

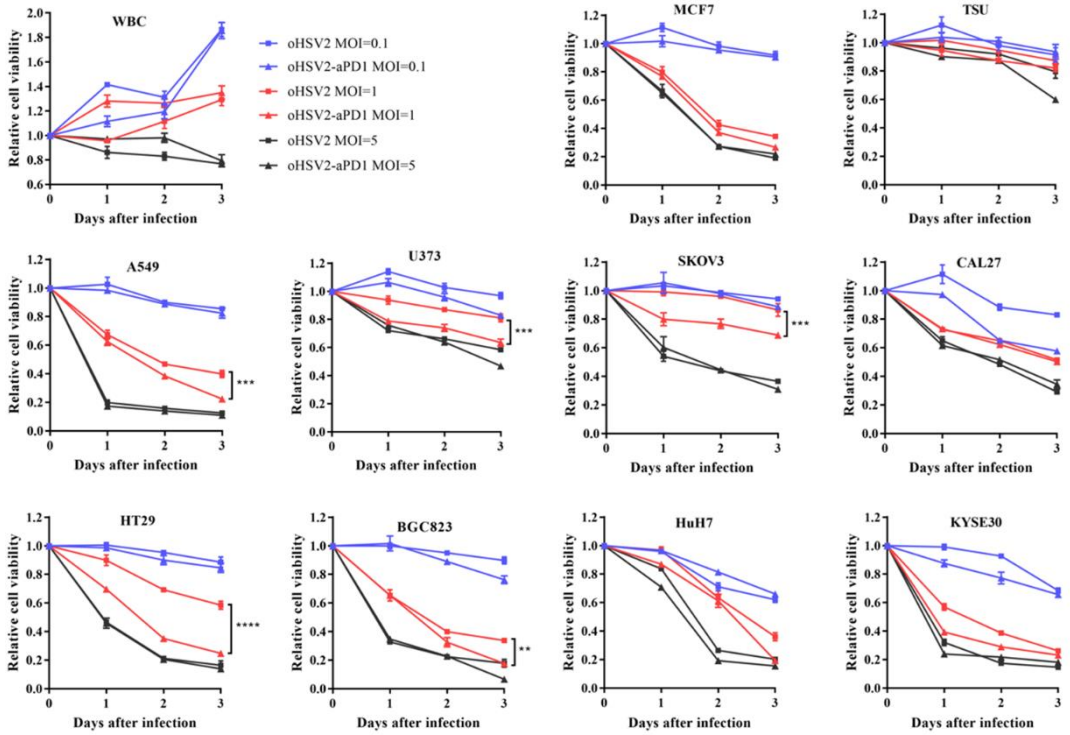

Figure Supplemental 4. Comparison of oncolytic activities of oHSV2 and oHSV2-aPD1 viruses in human cells

oHSV2 or oHSV2-aPD1 were used to mock-infect or infect WBC, TSU, MCF7, A549, U373, SKOV3, CAL27, HT29, BGC823, HuH7 and KYSE30 cells at the indicated three MOIs for the indicated lengths of time. Each value is presented as the mean ± SD of three measurements. Statistical significance is indicated by **($p < 0.01$), ***($p < 0.001$) and ****($p < 0.0001$).

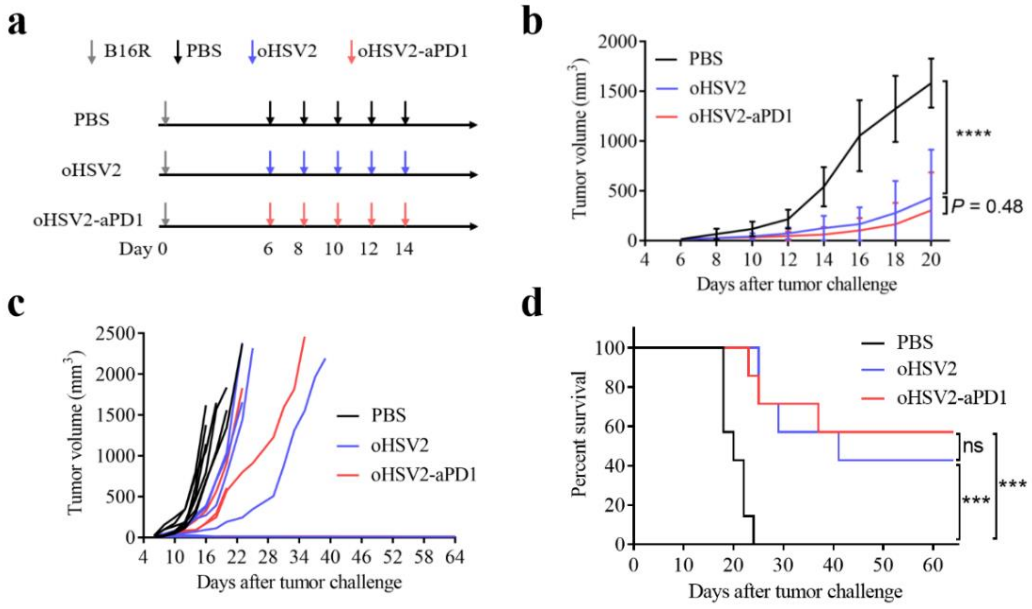

Figure Supplemental 5. Comparison of therapeutic effects of oHSV2 and oHSV2-aPD1 viruses in B16R melanoma model in normal C57BL/6J mice

Mice were subcutaneously inoculated with B16R cancer cells and treated via intratumoral injection as described in the Methods section (n = 7 per group). **(a)** Schematic representation of the experiment. **(b)** Tumor volumes within different groups were measured every other day and data are presented as the mean ± SD. **(c)** Tumor volumes from each specimen are shown individually. **(d)** Overall survival is shown using Kaplan-Meier curves and was analyzed using the Log rank test. (***$p < 0.001$, ****$p < 0.0001$, ns, not significant)

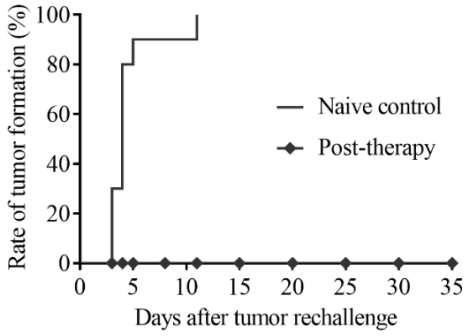

Figure Supplemental 6. Administration of oHSV2 and PD-1 antibody alone or their union led to an antitumor immune memory

Ten tumor-free mice from the four kinds of immunotherapies (anti-PD1, n = 1; oHSV2, n = 2; oHSV2-aPD1, n = 4; oHSV2 + anti-PD1, n = 3) were rechallenged at day 64 after the first tumor inoculation, with 2×10^5 B16R cells per mouse in the contralateral flank. And ten naive C57BL/6J-Pdcd1 mice received same dose tumor cells as a control.

Table Supplemental 1. Patient characteristics.

Patient ID	Age (year)	Gender	Type	TNM stage	Treatment
Patient RCC1	50	Male	[a]RCC	T3NxM1	None
Patient HCC1	59	Male	[b]HCC	TxN0M1	None
Patient CRC1	55	Male	[c]CRC	T3N2M0	Radiotherapy
Patient CRC2	55	Female	CRC	T3N1M0	None
Patient CRC3	65	Female	CRC	T3N2M1	Chemotherapy
Patient NSCLC1	84	Female	[d]NSCLC	T2N3Mx	None
Patient NSCLC2	61	Male	NSCLC	T2N2Mx	None
Patient NSCLC3	79	Male	NSCLC	T2N2M1	None

[a]RCC: renal cell carcinoma, [b]HCC: hepatocellular carcinoma, [c]CRC: colorectal cancer, [d]NSCLC: nonsmall cell lung cancer.